Effect of surface pinning on magnetic nanostuctures

Aditi Sahoo,[1] Dipten Bhattacharya,[1] and P. K. Mohanty[2,3]
[1]*Advanced Mechanical and Material Characterization Division, CSIR-Central Glass and Ceramic Research Institute, 196, Raja S.C Mullick Road, Kolkata, 700032 India*
[2]*Department of Physical Sciences, IISER Kolkata, Mohanpur, West Bengal 741246, India*
[3]*CMP Division, Saha Institute of Nuclear Physics, HBNI, 1/AF Bidhan Nagar, Kolkata, 700064 India*

(Received 25 September 2019; revised manuscript received 10 December 2019; accepted 27 January 2020; published 14 February 2020)

We show that pinning of surface spins affects the hysteresis properties of the core-shell magnetic nanostuctures of different shapes, sizes, and different spin interactions, namely, Ising, XY, and Heisenberg models. The asymmetry in hysteresis loops occuring due to pinning turns out to be more prominent in an inverse core-shell structure where spin interaction in the core is antiferromagnetic and that in the shell is ferromagnetic. Monte Carlo simulations of the inverse core-shell nanostructures show that the exchange bias, even under zero-field-cooled conditions, increases with increase of both the pinning density and the fraction of up spins among the pinned ones. The exchange bias also exhibits a switch—from negative to positive—depending on the fraction of up spins pinned. These results are remarkably well reproduced by a simple model of the outermost surface layer. The surface spin pinning appears to affect the magnetic properties of heterostructures as well, besides nanostructures.

DOI: 10.1103/PhysRevB.101.064414

I. INTRODUCTION

Nanoscale magnetic structures continue to attract tremendous attention from researchers because of the array of unusual properties as well as the ever-increasing application potential in magnetic recording [1,2], imaging [3], sensors (as well as smart) [4], DNA separation [5], magnetotransport [6], and targeted drug delivery devices [7,8]. While ferromagnetism could be stabilized in nanoparticles by dispersing them within an antiferromagnetic matrix and using, as a consequence, the exchange coupling interaction across the nanoparticle-host matrix interface [9], superspin glass [10] to superferromagnetism [11] could also be observed within different assemblages of nanoparticles because of esoteric exchange interactions. The magnetic properties such as saturation and remnant magnetization, coercivity, and exchange bias field (if any) also exhibit unusual features depending on particle size [12,13], shape [14], chemical composition [15], and crystallographic structure [16]. For instance, magnetization does not exhibit saturation even at higher applied fields ($>$ 50 kOe) in ferromagnetic nanosized particles [17]; coercivity and exchange bias also exhibit dependence on applied field and temperature [18,19]. Exchange bias could be observed even after zero field cooling from above the transition temperature [18,20]. The spin composites, forming within different platforms of nanomagnetic systems, could be comprised of a variety of structures such as ferromagnetic-antiferromagnetic [21], ferromagnetic-spin glass [22], ferrimagnetic-spin glass, ferrimagnetic-antiferromagnetic, etc. [23,24]. Complete exposition of the plethora of such structures and the structure-property correlation, therefore, is extremely difficult yet rewarding. Distilling the experimental and theoretical work carried out so far on nanomagnetic systems, it appears that the key factors, which govern the magnetic properties, are intra- and interphase exchange coupling interactions [25,26], magnetic anisotropies [27], and spin pinning at the interface [28] or at the surface [29]. Issues such as field, temperature, measurement protocol, thermal and field cycling dependence of magnetic properties observed in a score of nanomagnetic structures still defied complete description. An important factor in this context, hitherto not well considered, is the pinning of surface spins by defects. Nanosized magnetic particles—coated by organic liquid and thereby functionalized—were shown to exhibit incomplete saturation and spins, making large angles with the direction of the applied field [17].

We show in this paper that pinning density and the fraction of $\uparrow$ and $\downarrow$ surface spins pinned influence the magnetic properties far more strongly than the exchange coupling interactions. The magnetic properties have been calculated from Monte Carlo simulations for two- and three-dimensional systems (including heterostructures) and as a function of particle size and shape using different spin-spin interactions such as Ising, XY, and Heisenberg. Both the core shell (where the core is ferromagnetic and shell is antiferromagnetic) and inverse core-shell (where the core is antiferromagnetic and shell is ferromagnetic) nanostructures were considered. The variation of coercivity and exchange bias has been mapped as a function of pinning density, ratio of $\uparrow$ and $\downarrow$ spin fraction, core-shell thickness, and different shapes: elliptical, square, triangular and some irregular shapes. A simple model of the outermost surface layer with pinned spins is introduced and solved analytically; the interesting observations of the effect of surface pinning on a two-dimensional core-shell structure can be understood very well from this simple model. Interestingly, switch in exchange bias—from positive to negative—could be observed depending on variation in fraction of $\uparrow$ and $\downarrow$ spin

fractions. These results have very important ramifications for a range of experimental observations.

The paper is organized as follows. The model of the core-shell magnetic nanostructure is introduced in Sec. II and the simulation methods are discussed here. In Sec. III we study the core-shell structures in two dimensions and discuss how the hysteresis loops vary with change in interaction strengths, pinning parameters, shape, and size of the system. Similar results are obtained in three dimensions in Sec. IV, with Ising, XY, or Heisenberg models. We introduce a simple model of the outermost surface layer in Sec. V to understand why pinning affects hysteresis. Since pinning strongly alters the magnetic properties in mesoscopic scale, heterostructures in nanoscale are no exception; this is discussed briefly in Sec. VI. Finally, we summarize the results and conclude in Sec. VII.

II. THE MODEL AND SIMULATION

We intend to study the magnetic properties of core-shell nanostructures, primarily the nanoparticles. We consider that the nanoparticles have a core $\mathcal{C}$ and a shell $\mathcal{S}$. The Hamiltonian of the system is given by

$$\mathcal{H} = -J_c \sum_{i\in\mathcal{C}, j\in\mathcal{C}} \mathbf{S}_i.\mathbf{S}_j - J_{\rm sh} \sum_{i\in\mathcal{S}, j\in\mathcal{S}} \mathbf{S}_i.\mathbf{S}_j - J_{\rm int} \sum_{i\in\mathcal{S}\, j\in\mathcal{C}} \mathbf{S}_i.\mathbf{S}_j - H \sum_{i\in\mathcal{C}, i\in\mathcal{S}} S_i^x, \quad (1)$$

where j is the nearest neighbor of site i, J_c ($J_{\rm sh}$) is the exchange interaction among the spins within the core (shell), $J_{\rm int}$ represents core-shell interface interaction, and H is the external magnetic field. Obviously, the spins interact ferromagnetically (antiferromagnetically) when the corresponding value of interaction strength is positive (negative); for example, when $J_c < 0$ and sites i and j are within the core ($i \in \mathcal{C}$ and $j \in \mathcal{C}$), the spins $\mathbf{S_i}$ and $\mathbf{S_j}$ interact antiferromagnetically. The magnetic field H is experienced by all the spins, both in core $\mathcal{C}$ and shell $\mathcal{S}$, and its direction is taken as the x axis.

Note that when $J_c = J_{\rm sh} = J_{\rm int}$, Eq. (1) describes Ising, XY, or Heisenberg models on a lattice in any spatial dimension. The spin $\mathbf{S}_i$ at lattice site i is a unit vector, i.e., $\mathbf{S}_i.\mathbf{S}_i = 1$; for the Heisenberg model, $\mathbf{S}_i = (S_i^x, S_i^y, S_i^z)$ has three components and for the XY model, $\mathbf{S}_i = (S_i^x, S_i^y)$ has two components. To describe the Ising model, one must consider that $\mathbf{S}_i \equiv S_i^x = \pm 1$ and the dot product in Eq. (1) are interpreted as a simple multiplication of scalars. Thus, the core-shell structure emerges due to spatial inhomogeneity of interaction strength.

In addition, to model the surface pinning that has been observed in magnetic nanoparticles in contact of organic liquids [17], in ferromagnetic thin films [30], and core-shell structures [29], etc., we assume that η fraction of boundary spins are pinned. We also introduce a parameter $0 \leqslant r \leqslant 1$, which controls the fractions of pinned spins which are oriented along the field.

We must mention that usually magnetic materials have an easy axis $\hat{e}$ which contributes an additional magnetic anistropic energy term $\sum_i (\mathbf{S}_i.\hat{e})^2$ to the Hamiltonian. Such anisotropy alone cannot *generate* exchange bias at zero-field-cooled conditions, but it may have some influence on it. Since our focus here is to study whether exchange bias can be originated solely from pinning of surface spins, we avoid this anisotropic term.

Monte Carlo simulations

We study the hysteresis properties of the core-shell nanostructures using Monte Carlo simulations and single-spin Metropolis algorithm where a trial configuration is accepted with probability $\min\{1, e^{-\beta\Delta E}\}$; ΔE is the energy difference between the current and the trial configuration. The trial configuration is constructed by reorienting a single spin, chosen randomly; for the Ising model, the spin is flipped, whereas for XY and Heisenberg spins, the angles are changed by a small amount, chosen from a uniform distribution.

To measure hysteresis, first we set the temperature of the system to a fixed value smaller than critical temperature T_c. This can be achieved from any random initial configuration by relaxing the system for a long time, in zero-field-cooled conditions. Then we raise the magnetic field slowly from $H = 0$ to $H_{\rm max}$ with a field sweep rate ΔH units per Monte Carlo sweep (MCS) and, finally, the hysteresis loop calculations are undertaken for a cycle, by varying the field from $H_{\rm max}$ to $-H_{\rm max}$ and then to $H_{\rm max}$ again with same rate. Magnetization of the system is measured after each MCS and it is averaged over 100 samples. Random numbers are generated by using a standard linear congruential generator *drand48()*.

It is well known that the area of hysteresis and the coercive field depends strongly on the rate at which the field is swept [31]. The quasistatic field sweep in real systems (Tesla/second) translates to a rate of the order 10^{-12} units of magnetic field per MCS, which is not practically feasible in simulations. Instead, we choose a faster field sweep rate $\Delta H \sim 10^{-2}$ which may lead to overestimation of the coercive field but it keeps the value of exchange bias and the qualitative behavior of the coercive field unaltered. It is also advantageous for doing fast calculations. One must, however, note that a fast sweep rate must be associated with a large $H_{\rm max}$ to make a closed hysteresis loop; for $\Delta H \sim 10^{-2}$, the required field is typically of the order unity.

We primarily focus on the dependence of coercive field (H_c) and exchange bias field ($H_{\rm eb}$) on η, r, interface interaction strength $J_{\rm int}$, and size of the core and the shell. H_c and $H_{\rm eb}$ in a hysteresis loop are defined as

$$H_c = \tfrac{1}{2}(H_{c2} - H_{c1}) \quad \text{and} \quad H_{\rm eb} = \tfrac{1}{2}(H_{c2} + H_{c1}), \quad (2)$$

where H_{c2} and H_{c1} are the fields corresponding to zero magnetic moment in the forward and reverse branches of the hysteresis loop. Usually, for simple magnets, the coercive field H_{c1} is negative, H_{c2} is positive, and $|H_{c1}| = |H_{c2}|$ and thus $H_{\rm eb} = 0$. A positive (negative) exchange bias can occur in special situations when $|H_{c1}| < |H_{c2}|(|H_{c1}| > |H_{c2}|)$. In the following, we see that surface pinning can produce nonzero exchange bias in core-shell magnetic nanoparticles.

III. CORE-SHELL STRUCTURES IN TWO DIMENSIONS

Models in two dimensions are far from realistic three-dimensional core-shell structures, but they provide very good insight and better analytical understanding of the physical phenomena at hand. The exact solution of the model which

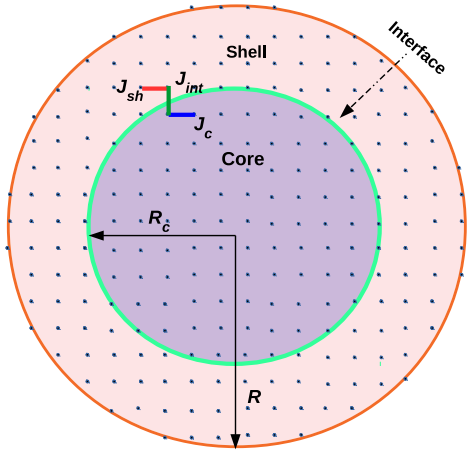

FIG. 1. Schematic representation of the core-shell structure: The core-shell structure in two dimensions is represented here by a square lattice bounded by a circle of radius R, within which there is a circular core having radius $R_c < R$; the annular region of width $R - R_c$ is the shell. Ising spins $s_i = \pm 1$, on the lattice sites belonging to the core (shell) interact with strength J_c ($J_{\rm sh}$) and the interaction strength across the interface is $J_{\rm int}$.

mimics only the outermost layer (in Sec. V) of the core-shell structure explicitly shows that the spin pinning generates an additional effective magnetic field in the system, leading to asymmetric hysteresis. Thus it is natural to expect that qualitative behavior of $H_{\rm eb}$ and H_c are same in Ising, XY, Heisenberg models; the actual value of the effective magnetic field, and that of H_c and $H_{\rm eb}$, depends on the details of the surface topology and the spin types. From a computational point of view, studying Ising model has an obvious advantage as it allows a phase transition in two dimensions, which cannot take place in models having continuous symmetry (XY or Heisenberg models) [32]. Taking this advantage into account, we study the two-dimensional core-shell structure in detail. A generalization to three dimensions is straightforward, which we discuss briefly in Sec. IV.

The core-shell structure can be obtained in two dimensions by considering a square lattice with circular boundaries of radius R, which has a circular core $\mathcal{C}$ of radius $R_c < R$; the shell region $\mathcal{S}$ falls between these two circles (see Fig. 1). Each lattice site i of this core-shell structure is associated with a spin $\mathbf{S}_i^x \equiv s_i = \pm 1$ (representing $\uparrow, \downarrow$) which interacts with other spins following Eq. (1). The Hamiltonian in Eq. (1) can be written as

$$\mathcal{H} = -J_c \sum_{i\in\mathcal{C}, j\in\mathcal{C}} s_i s_j - J_{\rm sh} \sum_{i\in\mathcal{S}, j\in\mathcal{S}} s_i s_j - J_{\rm int} \sum_{i\in\mathcal{S} j\in\mathcal{C}} s_i s_j - H \sum_{i\in\mathcal{C}, i\in\mathcal{S}} s_i. \quad (3)$$

We assume that η fraction of boundary spins are pinned, of which r fractions are oriented along H, i.e., the pinning density is η and the $\uparrow$-spin fraction (among pinned ones) is r.

A. Antiferromagnetic core and ferromagnetic shell

Let us proceed by assuming the interaction of spins within the core is antiferromagnetic ($J_c < 0$) whereas the interaction of spins in the shell is ferromagnetic ($J_{\rm sh} > 0$) and the interaction at the interface can be ferro- or antiferromagnetic; this is not the usual scenario but observed in several experimental systems [33]. We briefly discuss other possible structures in Sec. III B. In the following, we primarily study the hysteresis effects, particularly the dependence of coercive field and exchange bias on different model parameters and the shape and size of the core-shell structure.

For carrying out the Monte Carlo simulations, we consider the following default values for model parameters, unless otherwise specified:

$$R = 32, R_c = 26, \eta = 0.4, r = 0.7,$$
$$J_c = -0.5, J_{\rm sh} = 1, J_{\rm int} = 1. \quad (4)$$

The magnetic field is swept with rate $\Delta H = 0.02$ per MCS and with this rate, we need a high magnetic field $H_{\rm max} = 2$ to complete the hysteresis loop. Temperature of the system $\beta^{-1} = 1$ is kept fixed throughout the simulation [34].

1. *Dependence of $H_{\rm eb}$, H_c on η*

First we study the hysteresis properties of a nanoparticle by changing the pinning density η. Other parameters are kept fixed at the default values given in Eqs. (4). In Fig. 2(a), we present hysteresis loops for different η. These loops show negative exchange bias which increases as the pinning density η is increased. The exchange bias is maximum when all the spins are pinned at the surface. The reason for the asymmetry in the loop is that 70% of the pinned spins are $\uparrow$ and thus one requires some additional magnetic field to completely reverse the magnetization. The coercivity, however, decreases with increase of η. This is because, with increase in pinning density, more spins of ferromagnetic shell are pinned and a fewer number of spins of the shell take part in the hysteresis dynamics which effectively decreases the shell width.

2. *Dependence of $H_{\rm eb}$, H_c on r*

Different external conditions pin the spins on the surface differently. If the pinning is due to surface functionalization by organic solvent, both the density of pinned spins and the $\uparrow$-spin fraction may vary in different solvent conditions. Here we intend to change $\uparrow$-spin fraction r and investigate the hysteresis properties. For $r > \frac{1}{2}$, more $\uparrow$ spins are pinned compared to $\downarrow$ and one expects that an effective positive intrinsic field is generated in the system. Thus, one needs some additional negative external magnetic field to overcome this effect, resulting in a negative exchange bias. Similarly, a positive exchange bias is expected for $r < \frac{1}{2}$. In Fig. 2(b), we have plotted the hysteresis curves for different r, keeping $\eta = 0.4$ and other parameters the same as in Eqs. (4). The inset here shows dependence of $H_{\rm eb}$ and H_c on r. As expected, $H_{\rm eb} = 0$ for $r = \frac{1}{2}$; it is negative (positive) for $r > \frac{1}{2} (r < \frac{1}{2})$ and $|H_{\rm eb}|$ increases as one moves away from $r = \frac{1}{2}$. The coercivity, which primarily depends on the pinning density η, is almost independent of r.

3. *Dependence of $H_{\rm eb}$, H_c on $J_{\rm int}$*

We now study the influence of $J_{\rm int}$, the interface interaction strength. The hysteresis loops for particles with size $R = 32$

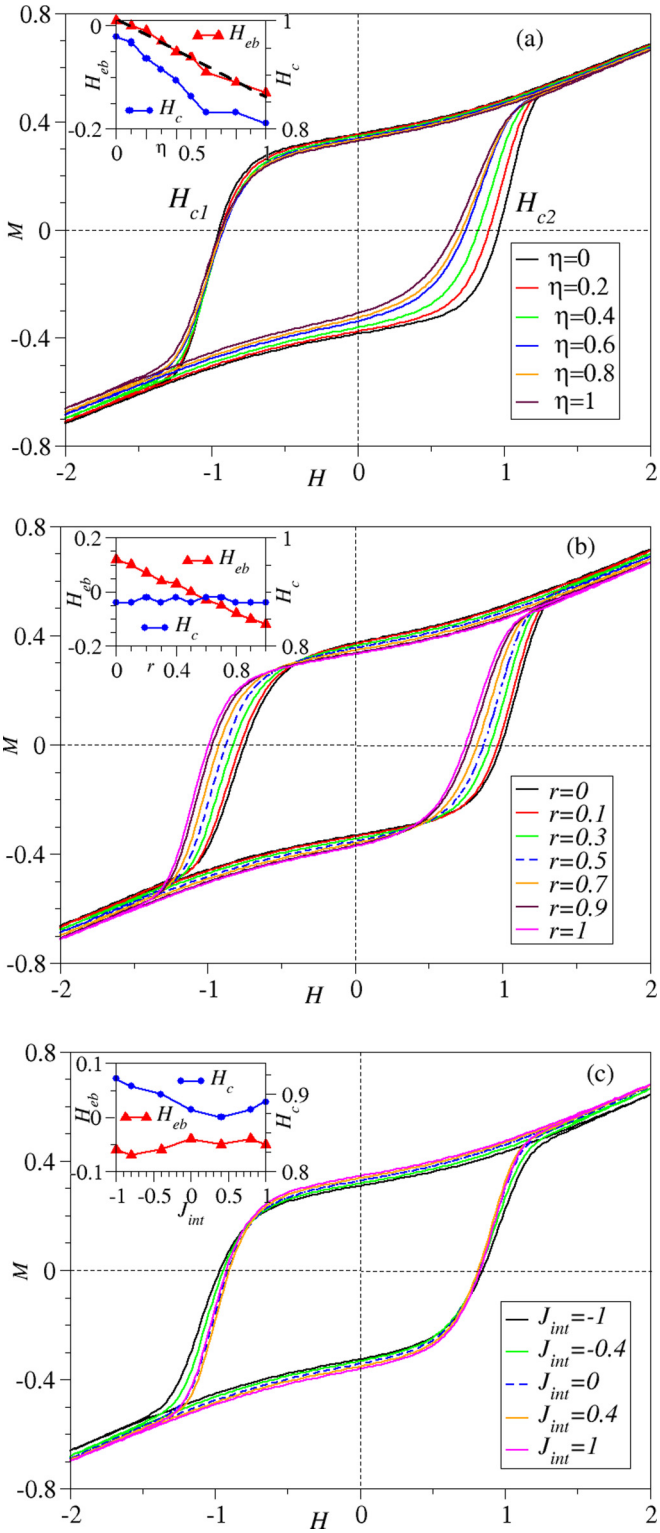

FIG. 2. The main figures show hysteresis loops for a two-dimensional circular core-shell structure when one of the model parameters X is changed while other parameters are taken from Eqs. (4); insets show the corresponding change in coercivity H_c and exchange bias $H_{\rm eb}$. (a) $X = \eta$: H_c decreases, but $|H_{\rm eb}|$ increases with increase of η. The dashed line is the best linear fit: $H_{\rm eb} = -0.15\eta + 0.013$. (b) $X = r$: H_c is almost a constant, but $|H_{\rm eb}|$ increases linearly with increase of η. (c) $X = J_{\rm int}$: No appreciable change in H_c and $|H_{\rm eb}|$.

and $Rc = 26$ are plotted in Fig. 2(c). With change of $J_{\rm int}$ we do not find any significant change in H_c and $H_{\rm eb}$; two extreme values $J_{\rm int} = 1, -1$ give rise to a slightly increased coercive field, but the exchange bias changes only a little. Thus, it appears that in a core-shell magnetic system, the exchange bias can be controlled effectively by the ↑-spin pinning fraction r and the pinning density η, not by the interface interaction $J_{\rm int}$.

One should note that some earlier studies have reported a significant change in exchange bias with change in interface interaction strength $J_{\rm int}$ [26]. These studies primarily focus on core-shell structures with a ferromagnetic core and antiferromagnetic shell [25,35,36], modeled by the usual Heisenberg model in three dimensions along with additional magnetic anisotropy [35,36] and sometimes in the presence of a crystal field [37]. In addition, hysteresis is studied in both field-cooled and zero-field-cooled conditions; the exchange bias and its change with respect to interface interactions are found to be significant only in field-cooled conditions [26].

In the present paper, we consider an inverse core-shell structure, with an antiferromagnetic core and ferromagnetict shell modeled by Ising spins in two dimensions and no magnetic anisotropy or any crystal field; in this simple case, even in zero-field-cooled conditions we find a large exchange bias $H_{\rm eb}$ when surface spins are pinned. $H_{\rm eb}$ will, of course, increase further in field-cooled conditions. To emphasize that surface pinning indeed causes large exchange bias, we extend the study to three-dimensional inverse core-shell structures, considering Ising, XY, and Heisenberg models (see Sec. IV); in all these cases, under zero-field-cooled conditions, the influence of $J_{\rm int}$ on $H_{\rm eb}$ is found to be negligible.

4. Dependence of $H_{\rm eb}$, H_c on R and R_c

Figure 3(a) shows the hysteresis loops of inverted core-shell structures for different R_c, keeping $R = 32$ fixed; thus the shell thickness increases with decrease in R_c. The other parameters are chosen from Eqs. (4). In Fig. 3(a), we plot the variation of coercive field and exchange bias with R_c. Here, $|H_{\rm eb}|$ increases with an increase in R_c and reaches a constant value asymptotically. The saturation magnetization and coercive field, however, decreases for larger R_c. This is because the coercivity primarily gets a contribution from the ferromagnetic shell (antiferromagnetic core produces zero net magnetic moment) whose thickness decreases with increased R_c.

It is important to ask whether the observed behavior is scalable, i.e., whether the asymmetric hysteresis survives in the thermodynamic limit where R_c and R increases, keeping their ratio fixed. To study this, we increase particle size R while increasing the core size R_c proportionately, $R_c = \frac{3}{4}R$. Other parameters are shown in Fig. 3(a). We find [Fig. 3(c)] that the size of the hysteresis loop increases with R as the number of ferromagnetic layers are increased. This is reflected in an increased value of coercivity in Fig. 3(d). However, the magnitude of the exchange bias $|H_{\rm eb}|$ decreases with R, indicating the decrease in asymmetry of the loop with R and the usual symmetric hysteresis loop in the thermodynamic limit. Thus, the exchange bias due to surface pinning is only the mesoscopic effect, which goes away in larger systems when surface-to-volume ratio becomes very small. In fact, similar

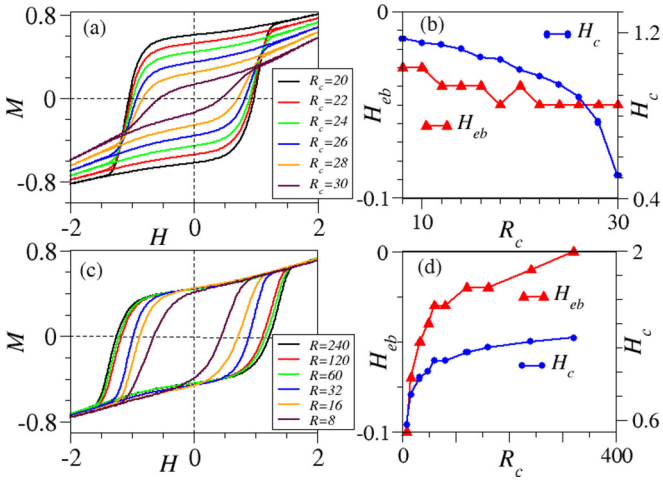

FIG. 3. (a) Hysteresis loops for different shell thicknesses $R - R_c$, obtained by varying R_c, keeping $R = 32$ fixed. (b) $|H_{\rm eb}|$ increases with increased R_c and reaches a constant for large R_c. H_c also decreases with increase of R_c, as the number of ferromagnetic layers also decrease. (c) The thermodynamic limit of the system can be achieved by changing the size of the core and shell proportionately. Here we plot hysteresis loops for different R and fixed $\frac{R_c}{R} = \frac{3}{4}$. (d) H_c, $H_{\rm eb}$ as a function of R. H_c increases with R as the number of ferromagnetic layers increase. However, $H_{\rm eb} \to 0$ because the surface- (where pinning occurs) to-volume ratio approaches zero in the thermodynamic limit. Unspecified parameters here are taken from Eqs. (4).

size dependence of coercivity and $H_{\rm eb}$ has been observed in systems with a ferromagnetic shell and antiferromagnetic core [33,38].

B. Ferromagnetic core or antiferromagnetic shell

The core-shell structure that we studied so far has ferromagnetic interaction in the shell and antiferromagnetic interaction in the core. We have investigated the other possibilities too. The influence of surface pinning turned out to not be that prominent when the core (shell) is ferromagnetic (antiferromagnetic) irrespective of the interaction in the shell (core). We decided not to present these studies in detail as these results neither add any significant information nor alter the conclusions of this paper.

When spins interact ferromagnetically in the shell, the pinning of surface spins (which belong to the shell) can produce an effective additional magnetic field which in turn generates an asymmetry in the hysteresis loop. On the other hand, when spin interactions in the shell are antiferromagnetic, the pinning is less effective as other spins in the shell can orient in a direction opposite to the pinned spins and make an antiferromagnetically ordered structure throughout; thus, the effective intrinsic field produced in the system is negligible. In this case, some sites might encounter frustrations and may give rise to certain local residual magnetic moments, but the number of the frustrated spins are statistically very small. On the other hand, when the core is ferromagnetic, one generally gets large hysteresis loops even in the absence of surface pinning because the volume of the core is usually much larger compared to that of the shell. Thus, the relative change of exchange bias and coercivity produced by surface pinning is quite small.

In summary, surface pinning surely affects the hysteresis properties in core-shell nanostructures but it is more prominent when interaction in the core is antiferromagnetic and that in the shell is ferromagnetic.

C. Different surface morphology

Like other nanomaterials [39], the surface morphology or shape of core-shell nanocomposites may be changed. Morphology of the nanoparticle can be spherical [40], square [38], elliptical [41], triangular [42], or it may be irregular [43]. Their magnetic properties depend crucially on the surface anisotropy [44]. Other properties like catalytic activity, electrical, and optical properties are also highly shape dependent [45]. Combination of core-shell materials in different dimensions and shapes are designed regularly for their potential application in technology, like magnetoplasmonic applications, [46], and fluorescence applications [47]. In this section, we have studied hysteresis properties of two-dimensional core-shell nanostructures having different shapes.

To emphasize how *change in surface morphology* affects the magnetic properties, we did Monte Carlo simulation of core-shell nanoparticles of different shapes, but similar area and shell thickness. Coercivity and exchange bias obtained for different shapes are compared with those of the circular core-shell structure with $R = 32$ and $R_c = 26$.

We consider four different shapes: (i) a triangular core-shell structure with base $a = 86$, (ii) a square core-shell structure with side $a = 56$, (iii) an elliptical core-shell structure with major axis $a = 46$ and minor axis $b = 23$, and (iv) a core-shell structure with irregular surface but circular core or radius $R_c = 26$. In all the cases except (iv), the shell thickness is taken to be six lattice units and for (iv) the average thickness is $\simeq 6$. The interaction parameters $J_c = -0.5$, $J_{\rm sh} = 1$, $J_{\rm int} = 1$ and the pinning parameters $\eta = 0.4$, $r = 0.7$ are kept the same. Hysteresis loops of all these different shapes, along with that of the circle, are plotted in Fig. 4. The coercive field of the circular shape is found to be maximum; then they are decreasing in order: circle, triangle, square, ellipse, and the irregular shape. The corresponding exchange biases are $H_{\rm eb} = -0.05, -0.06, -0.11, -0.08$, and -0.06 respectively.

1. Local magnetic structure

The local magnetic structure changes during the hysteresis cycle. We consider the spin configurations at four different positions in the hysteresis cycle, marked as $B_\pm$ and $F_\pm$ in Fig. 5, and averaged the configurations over 100 statistical samples to get the local magnetization profile $\{m_i\} = \{\langle s_i \rangle\}$. The positions $B_\pm$ ($F_\pm$) correspond to backward (forward) directions of the loop with $H = \pm 1$. The density plots of the magnetization profile, marking red (blue) as $m_i = 1 (m_i = -1)$ are shown in Fig. 5. Position B_+ (F_-) is near to the maximum (minimum) field $H_{\rm max}$ ($-H_{\rm max}$), where the moment values are preferably positive (negative); thus, the ferromagnetic shell regions are almost fully magnetized and appear as a dark red (blue) borders. At B_- (F_+) the antiferromagnetic core has relaxed to have a predominantly negative (positive) moment

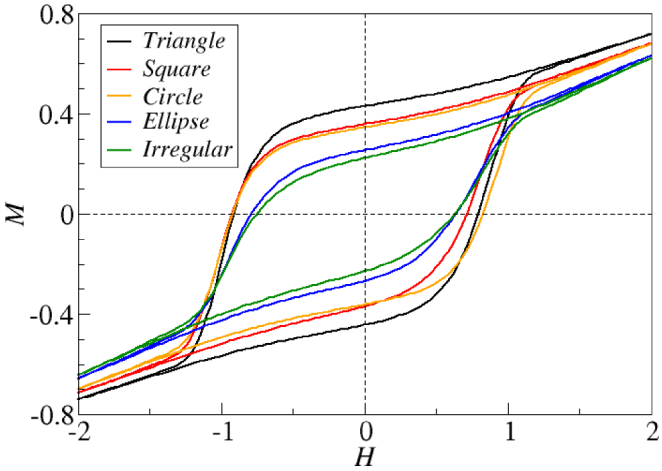

FIG. 4. Shape dependence of magnetic hysteresis of core-shell nanoparticles for (i) equilateral triangle (base $a = 86$), (ii) square ($a = 56$), (iii) circle ($R = 32$), (iv) ellipse (major and minor axis $a = 46$, $b = 23$), and (v) an irregular shape (core radius $R_c = 26$). Each one has approximately the same particle size and shell thickness. Corresponding $H_c = 0.86, 0.83, 0.89, 0.72, 0.7$ and $H_{\rm eb} = -0.06, -0.11, -0.05, -0.08, -0.06$. Unspecified parameters are taken as the default values given in Eqs. (4).

consistent with the field direction whereas the relaxation has not happened in the ferromagnetic shell, which is hysteretic.

2. *Aspect ratio*

We notice that the coercivity of the elliptical core-shell structure is smaller than that of the circular one with same

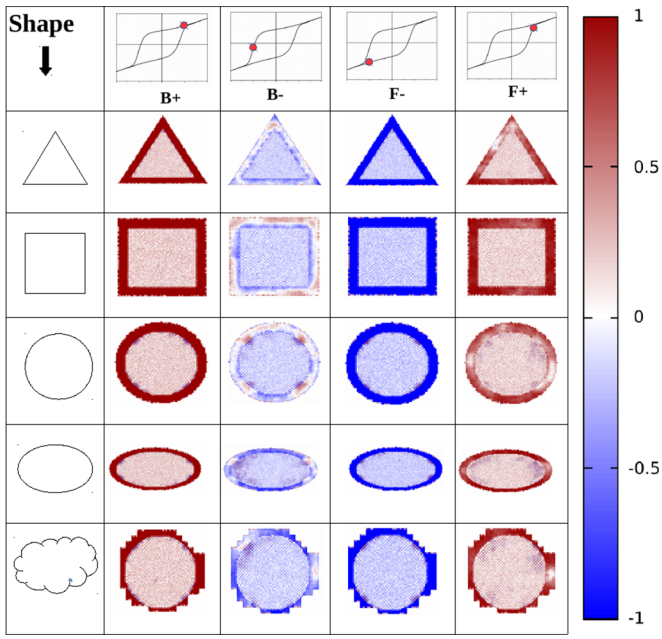

FIG. 5. Magnetization profile of inverse core-shell structure of different shapes at four different positions in hysteresis loop, each indicated by a •. Continuous variation of magnetization from −1 to 1 are colored as blue to red. All the model parameters are taken same as in Fig. 4.

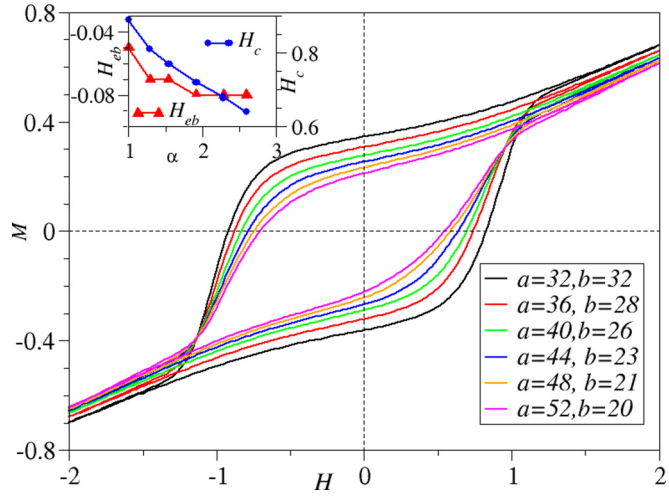

FIG. 6. Hysteresis loop of elliptic core-shell structures, with approximately same area but different aspect ratio $\alpha = a/b$. All other parameters are taken from Eqs. (4). The inset shows that the coercivity H_c decreases, but $|H_{\rm eb}|$ increases with α.

area. This indicates that a rodlike structure may have the smallest coercivity, which indeed has been observed earlier [14]. Here we aim at studying, systematically, how aspect ratio affects $H_{\rm eb}$ and H_c. To this end, we change the aspect ratio $\alpha = \frac{a}{b}$ of the ellipse and follow the change in its magnetic properties. Figure 6 shows the hysteresis loops; the coercivity and exchange bias are plotted in the inset as a function of the aspect ratio. The interaction parameters and the pinning parameters are taken same as earlier. Note, that the coercive field H_c decreases, but $|H_{\rm eb}|$ increases as the aspect ratio α increases.

IV. CORE-SHELL STRUCTURES IN THREE DIMENSIONS

In three spatial dimensions, magnetic phase transitions can occur in systems having discrete (Ising) or continuous spins (like XY and Heisenberg). In this section, we extend our study to core-shell structures with spin interactions given by either Ising, XY, or Heisenberg models. We study the hysteresis properties of three models, separately, on a cubical core shell with core $\mathcal{C}$ of length R_c and shell $\mathcal{S}$ of width $R - R_c$, i.e., we have a cubical core of size R_c^3 and particle size R^3.

We compare the hysteresis curves obtained from Monte Carlo simulations of all three models on a core-shell structure for $R_c = 26$ and $R = 32$, which means that the width of the shell is six lattice units. The interaction parameters are taken as $J_c = -0.5$, $J_{\rm sh} = 1$, $J_{\rm int} = 1$.

In Fig. 7, we have plotted the hysteresis curves for $\eta = 0.4$. The insets in Figs. 7(a) and 7(b) show, respectively, the variation of H_c and $H_{\rm eb}$ as a function of pinning density η. Here $r = 1$ (i.e., all pinned spins are oriented along the field), $H_{\rm max} = 4$, and the field sweep rate is $\Delta H = 0.04$. Clearly, in all three models, the coercivity H_c decreases with η, whereas, as expected, $|H_{\rm eb}|$ increases. For the Heisenberg model, both H_c and $|H_{\rm eb}|$ are quite high compared to those obtained from other models.

Asymmetric hysteresis, and thus large exchange bias, has been observed earlier in core-shell nanostructures. For the

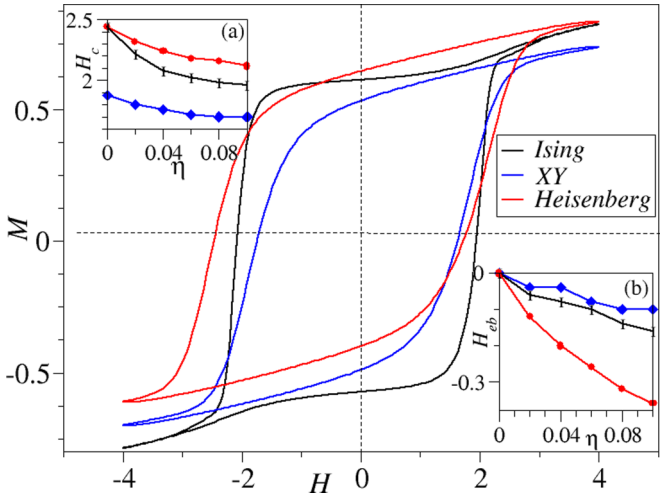

FIG. 7. Hysteresis loops of a cubical core-shell structure (particle size R^3 and core size R_c^3) for Ising, XY, and Heisenberg models, with $R_c = 26$, $R = 32$, pinning density $\eta = 0.1$, and interaction parameters $J_c = -0.5$, $J_{\rm sh} = 1$, $J_{\rm int} = 1$. The insets (a) and (b), respectively, show variation of H_c and $H_{\rm eb}$ as a function of η. Heisenberg models generate maximum $|H_{\rm eb}|$ and coercivity H_c.

ferromagnetic core and antiferromagnetic shell, one of the primary factors that controls the magnetic properties is the core-shell interaction parameter. Numerical studies of these core-shell structures with Heisenberg spin interactions, additional anisotropic spin interaction, and crystal field claims that, under field-cooled conditions, the exchange bias strongly depends on the nature and strength of core-shell interaction [25,26]. Here we show that surface pinning can affect the exchange bias strongly, even in zero-field-cooled conditions and in absence of anisotropy or crystal fields. This pinning effect is quite dominant in inverse core-shell nanostructures where the core is antiferromagnetic and the shell, ferromagnetic.

V. WHY PINNING AFFECTS HYSTERESIS

What we observe so far from the Monte Carlo simulation of the core-shell nanostructure is that, irrespective of shape, size, value of the interaction strength, and pinning parameters, the exchange bias $H_{\rm eb}$ increases with increase of pinning density η and decrease of $\uparrow$ spins fraction r. To understand this, we introduce a simple model of the surface by ignoring the interaction of the surface spins with those in the bulk (shell). In the two-dimensional core-shell structure of Ising spins, the surface is as a one-dimensional chain with periodic boundary conditions; the corresponding Hamiltonian is now

$$\mathcal{H}_{\rm surf} = -J_{\rm sh}\sum_{i=1}^{L} s_i s_{i+1}, \tag{5}$$

where L is total number of spins on the surface. For a circular core-shell structure studied here, $L \simeq 2\pi R$; in fact, a better approximation is $L \simeq 4R$, since for every $i \in (-R, R)$ there are two boundary spins. We assume that N spins on the surface are pinned, of which N_+ spins are $\uparrow$, thus $\sum_k S_k = 2N_+ - N = M_b$. Accordingly,

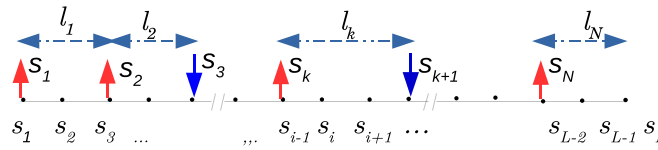

FIG. 8. The pinned spins are denoted $\{S_1, S_2, \ldots S_N\}$. Here $S_1 = s_1$, $S_2 = s_3, \ldots S_N = s_{L-2}$. Distance between two consecutive pinned spins S_k and S_{k+1} is l_k. The periodic boundary condition ensures that $s_{i+L} = s_i$ and $S_{k+N} = S_K$.

$$\eta = \frac{N}{L}, \quad r = \frac{N_+}{N} \quad \text{and} \quad m_b \equiv \frac{M_b}{N} = 2r - 1. \tag{6}$$

For notational convenience, let us denote the pinned spins as $\{S_1, S_2, \ldots S_N\}$ with $S_1 = s_{i_{\rm min}}$, where $i_{\rm min}$ is the position index of the first pinned spin (see Fig. 8). As shown in the figure, the separation of two consecutive pinned spins S_k and S_{k+1} is l_k.

The partition function of the system can be written as

$$Z_{L,N}(\{l_i\}) = \sum_{\{s_i\}} e^{-\beta\mathcal{H}_{\rm surf}} = \prod_{k=1}^{N}\langle S_k|T^{l_k}|S_k\rangle\,\delta\left(\sum_{k=1}^{N} S_k - M_b\right), \tag{7}$$

where $T = \begin{pmatrix} e^{K} & e^{-K} \\ e^{-K} & e^{K} \end{pmatrix}$ with $K = \beta J_{\rm sh}$ is the usual transfer matrix of one-dimensional Ising model, and $K = \beta J_{\rm sh}$.

In presence of the constraint, that exactly N_+ out of N pinned spins are $\uparrow$, which is ensured by a δ function in the above equation, evaluating this partition-sum Eq. (7) is difficult. We proceed to find a generating function of $Z_{L,N}(\{l_i\})$,

$$\mathcal{Z}_L(x) = \sum_{M_b=0}^{\infty} Z_{L,N}(\{l_i\})x^{M_b} = \mathrm{Tr}\left[\prod_{k=1}^{N}\left(AT^{l_k}\right)\right], \tag{8}$$

$$\text{where } A = \sum_{S_k=\pm} x^{S_k}|S_k\rangle\langle S_k| = \begin{pmatrix} x & 0 \\ 0 & x^{-1} \end{pmatrix}. \tag{9}$$

Eigenvectors of T are $|\pm\rangle = \begin{pmatrix} 1 \\ \pm 1 \end{pmatrix}$ with eigenvalues $\lambda_\pm = e^K \pm e^{-K}$, the generating function $\mathcal{Z}_L(x)$ can be evaluated using the diagonalizing matrix $U = \frac{1}{\sqrt{2}}\begin{pmatrix} 1 & 1 \\ 1 & -1 \end{pmatrix}$,

$$\mathcal{Z}_L(x) = \lambda_+^L\left(x + \frac{1}{x}\right)^N\left[1 + \left(\frac{\lambda_-}{\lambda_+}\right)^{l^*}\left(\frac{x^2-1}{x^2+1}\right)^2 + \ldots\right] \tag{10}$$

where, we have used $\sum_{k=1}^{N} l_k = L$ and $l^* = \min(\{l_i\})$ is the smallest separation between consecutive pinned spins.

Note that, for any given choice of separations $\{l_k\}$, one can calculate $\mathcal{Z}_L(x)$ explicitly using Eq. (10). In the second step here, we use a perturbation series in $\lambda = \frac{\lambda_-}{\lambda_+} = \tanh(\beta J_{\rm sh})$, valid quite well in the large temperature limit. The dominant (zeroth order) term of $\mathcal{Z}_L(x)$ does not depend on individual separations $\{l_k\}$, and the next order correction depends only on the smallest separation l^*. We have assumed that the smallest separation l^* appears only once in $\{l_k\}$; if it appears n times (and the separations are not adjacent to each other) then we

have an additional multiplicative factor n :

$$\mathcal{Z}_L(x) \simeq \lambda_+^L (x + x^{-1})^N \left[1 + n\lambda^{l^*}\left(\frac{x^2-1}{x^2+1}\right)^2\right]. \quad (11)$$

The average value of M_b is now

$$\langle M_b \rangle = x\frac{d}{dx}\ln \mathcal{Z}_L(x) = N\frac{x^2-1}{x^2+1} + \frac{4n\lambda^{l^*}x^2}{(1+x^2)^2 + n\lambda^{l^*}(x^4-1)}. \quad (12)$$

Note that the partition function $\mathcal{Z}_L(x)$ in Eq. (8) can be mapped to an Ising model on a one-dimensional periodic lattice,

$$\mathcal{H}_{\text{Ising}} = -J\sum_{i=1}^{L} s_i s_{i+1} - \sum_{i=1}^{L} H_i s_i \quad (13)$$

with inhomogenous magnetic field H_i acting at site i. The partition function is then,

$$\mathcal{Z}_{\text{Ising}} = Tr\left[\prod_{i=1}^{L}(A_i T)\right], \text{ where } T = \begin{pmatrix} e^{\beta J} & e^{-\beta J} \\ e^{-\beta J} & e^{\beta J} \end{pmatrix}$$

$$\text{and} \quad A_i = \begin{pmatrix} e^{\beta H_i} & 0 \\ 0 & e^{-\beta H_i} \end{pmatrix}. \quad (14)$$

Clearly, this equation becomes identical to the partition function of the pinned surface defined in Eq. (8) if (i) $H_i = h$ for all pinned sites and $H_i = 0$ for other sites, (ii) $J_{\text{sh}} = J$, and (iii) x in Eq. (9) is identified as $x = e^{\beta h}$.

The effective Hamiltonian is then

$$\tilde{\mathcal{H}}_{\text{surf}} = -J_{\text{sh}}\sum_{i=1}^{L} s_i s_{i+1} - h\sum_{k=1}^{N} S_k, \quad (15)$$

where the magnetic field h acts *selectively* only on the pinned spins.

Thus, a system having exactly N_+ number of $\uparrow$ spins among N pinned ones is equivalent to a system without pinning, but with an additional magnetic field h acting only on the pinned spins. The value of h for any given $r = \frac{N_+}{N}$ can be calculated from Eqs. (12) and (6) as

$$r = \frac{1}{2}\left(1 + \tanh(\beta h) + \frac{1}{N}\frac{n\lambda^{l^*}\,\text{sech}(\beta h)^2}{1 + n\lambda^{l^*}\tanh(\beta h)}\right). \quad (16)$$

In addition, when an external magnetic field H is applied to the system, the effective field per site becomes

$$H_{\text{eff}} = H + \eta h. \quad (17)$$

Thus, the hysteresis loops, which are symmetric when plotted against H_{eff}, would now appear asymmetric (shifted by a factor ηh) against the external field H. The exchange bias is then

$$H_{\text{eb}} = -\eta h. \quad (18)$$

To calculate h from Eq. (16) explicitly, let us consider the large N limit so the smallest separation between two consecutive spins is $l^* \simeq 1$. To a leading order in N,

$$h = \frac{1}{\beta}\tanh^{-1}(m_b) - \frac{1}{\beta N}\frac{n\lambda}{n\lambda m_b + 1}. \quad (19)$$

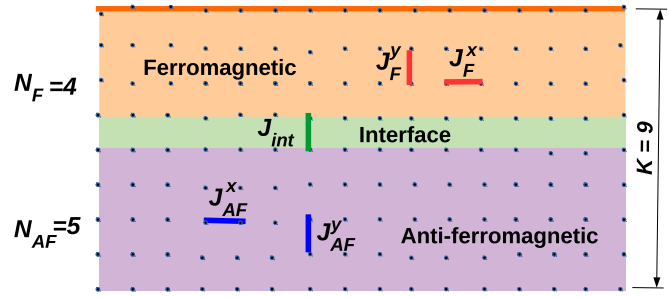

FIG. 9. Schematic representation of the heterostructure of K layers (each containing L sites) of which $N_{\text{AF}} = 5$ layer are antiferromagnetic and $N_{\text{F}} = 4$ ferromagnetic. The intra-layer coupling strengths in ferro and antiferro layers are respectively $J^x_{\text{F,AF}}$ and interlayer coupling strengths are $J^x_{\text{F,AF}}$. The interaction at the interface is J_{int}. Pinning of spins occur only at the top layer $k = K$.

The effective field h, along with Eq. (18), indicates that the exchange bias increases linearly, with pinning density η and temperature β^{-1}; it also grows monotonically with m_b or $r = \frac{1+m_b}{2}$. Linear dependence of H_{eb} on η, r are observed in Figs. 2(a) and 2(b), respectively.

It is interesting that a simple model of the surface which ignores the interaction of the surface spins with other spins in the shell completely reproduce the properties of hysteresis qualitatively.

VI. HETEROSTRUCTURES

Heterostructures are layered magnetic composites which, at nanoscale, may experience the influence of surface pinning [48]. We investigate the effect of pinning by modeling heterostructures as N_{F} number of ferromagnetic layers placed on the top of N_{AF} number of antiferromagnetic layers.

In two dimensions, the layers are line segments having L lattice sites labeled by $i = 1, 2, \ldots, L$.

We consider Ising spins on the heterostructure denoted by $s_i^k = \pm 1$ with two indices, a lattice site index $i = 1, 2, \ldots, L$, and a layer index $k = 1, 2, \ldots, K = N_{\text{AF}} + N_{\text{F}}$ (see Fig. 9). The intralayer interaction strength of Ising spins in ferromagnetic (antiferromagnetic) layers are J^x_{F} (J^x_{AF}), whereas the same in the interlayer are J^y_{F} (J^y_{AF}). At the interface, the interaction strength is J_{int}, which may be positive (ferro) or negative (antiferro). The corresponding Hamiltonian is

$$\mathcal{H} = -J^x_{\text{AF}}\sum_{k=1}^{N_{\text{AF}}}\sum_{i=1}^{L-1} s_i^k s_{i+1}^k - J^x_{\text{F}}\sum_{k=N_{\text{AF}}+1}^{K}\sum_{i=1}^{L-1} s_i^k s_{i+1}^k - J^y_{\text{AF}}\sum_{k=1}^{N_{\text{AF}}-1}\sum_{i=1}^{L-1} s_i^k s_i^{k+1} - J^y_{\text{F}}\sum_{k=N_{\text{AF}}+1}^{K-1}\sum_{i=1}^{L-1} s_i^k s_i^{k+1} - J_{\text{int}}\sum_{i=1}^{L-1} s_i^{N_{\text{AF}}} s_i^{N_{\text{AF}}+1} - H\sum_{k=1}^{K}\sum_{i=1}^{L} s_i^k. \quad (20)$$

We also consider that pinning of spins occurs only at the top (or exposed) layer $k = K$.

In Monte Carlo simulations (single spin Metropolis), starting from a random initial configuration at temperature $\beta^{-1} = 1$ we first increase the field from $H = 0$ to $H = H_{\text{max}} = 2$ with

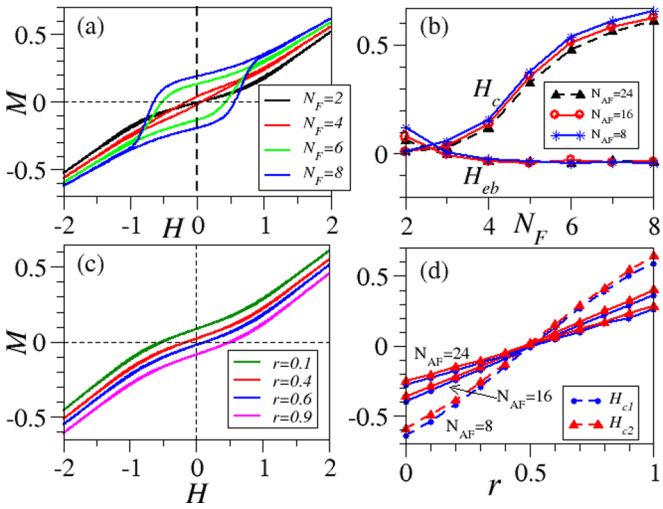

FIG. 10. (a) Hysteresis loop of two-dimensional heterostructures of N_F ferromagnetic layers on the top of $N_{AF} = 24$ antiferromagnetic layers. Here the length of each layer is $L = 128$, ↑-spin fraction $r = 0.6$. Corresponding values of H_c and H_{eb} are shown as a dashed line in (b); similar curves of H_c and H_{eb} as a function of N_F, for $N_{AF} = 16, 8$ are also shown there (solid lines). (c) Hysteresis curves for different r, for a heterostructure with $N_{AF} = 8$ and $N_F = 2$. The corresponding values of H_{c1} and H_{c2} as a function of r, are shown (dashed line) in (d). The solid lines in (d) show variation of H_{c1}, H_{c2} for different $N_{AF} = 16, 24$. The unspecified parameters here are same as in Eqs. (4).

a sweep rate 0.01 units per MCS. The zero-field hysteresis cycle is performed by varying the field from $H = 2$ to $H = -2$, and then back to $H = 2$.

First, we calculate the variation of coercivity H_c and exchange bias H_{eb} by varying the number of ferromagnetic layers N_F for a fixed number of $N_{AF} = 24$, as shown in Fig. 10 (a). The interaction parameters are taken to be $J^x_{AF} = J^y_{AF} = J_{AF} = -0.5$, $J^x_F = J^y_F = J_F = 1$. At the interface, we have $J_{int} = 1$. The pinning parameters are the pinning density $\eta = 0.4$ and the ↑-spin fraction $r = 0.6$. Corresponding H_c and H_{eb} are shown in Fig. 10(b) by a dashed line; the solid lines there correspond to $N_{AF} = 8, 16$. Clearly, the coercivity of the heterostructure decreases monotonically as N_F decreases.

We also find an interesting finite size effect: For all values of N_F, except for $N_F = 2$, the exchange bias H_{eb} is negative, as expected for $r > 0.5$. In fact, for $N_F = 2$, both H_{c1} and H_{c2} are positive. We further investigate heterostructures with $N_F = 2$, for different ↑-spin fraction and different N_{AF}. Figure 10(c) shows hysteresis curves for a heterostructure of $N_{AF} = 8, N_F = 2$ for different r; corresponding values of H_{c1} and H_{c2} are plotted in Fig. 10(d) by a dashed line. Similar plots for $N_{AF} = 16, 24$ (and $N_F = 2$) are shown in Fig. 10(d) with solid lines. Surprisingly, for $N_F = 2$, both H_{c1} and H_{c2} take the same sign irrespective of the number of antiferro layers: both are positive (negative) when $r > 0.5 (r < 0.5)$. Comparing the curves of $N_{AF} = 8, 16, 24$, it appears that this unusual finite size effect goes away slowly as N_{AF} increases. This is because for very large N_{AF} the interaction in the bulk is largely antiferromagnetic and one expects $H_{c1} = 0 = H_{c2}$.

VII. SUMMARY AND CONCLUSION

To summarize, we studied in detail the effect of surface pinning on magnetic properties of core-shell nanostructures and heterostructures in nanoscale using different spin-spin interactions such as Ising, XY, and Heisenberg. The effect of surface pinning turned out to be more prominent in an inverse core-shell structure where spins interact antiferromagnetically in the core and ferromagnetically in the shell. We study hysteresis by changing the interaction and pinning parameters in Monte Carlo simulations to conclude that the exchange bias increases with increase in pinning density and the fraction of ↑ spins pinned. This behavior could be reproduced remarkably from the analytical studies of a model introduced here that captures only the pinning and the spin-spin interaction in the outermost surface layer. The shape and size of the nanoparticles, which can be tuned experimentally, also strongly modify the exchange bias and coercivity.

We further investigate the nanoscale heterostructurs of ferrromagnetic layers grown on the top of antiferromagnetic layers. Spin pinning in the exposed ferromagnetic surface layer here produces an exchange bias similar to core-shell nanostructures. An interesting finite size effect is observed: it turns out that for a system with two ferromagnetic layers, both H_{c1} and H_{c2} takes the same sign, positive (negative) when ↑-spin fraction is greater (less) than $\frac{1}{2}$.

We believe that this mechanism of exchange bias generated from the pinning of spins on the surface, whose morphology and pinning density can be changed easily in experiments, will help in tuning the exchange bias for many fruitful technological applications in the future.

ACKNOWLEDGMENTS

A.S. acknowledges support from DST-INSPIRE in the form of a Senior Research Fellowship. P.K.M. acknowledges support from the Science and Engineering Research Board (SERB), India, Grant No. TAR/2018/000023.

[1] J. Jia, J. C. Yu, Y. X. J. Wang, and K. M. Chan, ACS Appl. Mater. Interfaces. **9**, 2579 (2010).
[2] C. T. Lo, Y. Watanabe, H. Oya, K. Nakabayashi, H. Mori, and W. C. Chen, Chem. Commun. **52**, 7269 (2016).
[3] H. Wang, A. Mararenko, G. Cao, Z. Gai, K. Hong, P. Banerjee, and S. Zhou, ACS Appl. Mater. Interfaces **6**, 15309 (2014).
[4] C. Goubault, P. Jop, M. Fermigier, J. Baudry, E. Bertrand, and J. Bibette, Phys. Rev. Lett. **91**, 260802 (2003).
[5] M. Tabuchi, M. Ueda, N. Kaji, Y. Yamasaki, Y. Nagasaki, K. Yoshikawa, K. Kataoka, and Y. Baba, Nat. Biotech. **22**, 337 (2004).
[6] J. M. Kinsella and A. Ivanisevic, J. Phys. Chem. C **112**, 3191 (2008).

[7] *Nanomagnetism: Fundamentals and Applications*, edited by Chris Binns (Elsevier, Netherlands, 2014).

[8] J. McCathy and R. Weissleder, Adv. Drug Deliv. Rev. **60**, 1241 (2008).

[9] V. Skumryev, S. Stoyanov, Y. Zhang, G. Hadjipanayis, D. Givord, and J. Nogués, Nature (London) **423**, 850 (2003).

[10] X. Chen, S. Bedanta, O. Petracic, W. Kleemann, S. Sahoo, S. Cardoso, and P. P. Freitas, Phys. Rev. B **72**, 214436 (2005).

[11] S. Bedanta, T. Eimüller, W. Kleemann, J. Rhensius, F. Stromberg, E. Amaladass, S. Cardoso, and P. P. Freitas, Phys. Rev. Lett. **98**, 176601 (2007).

[12] G. C. Papaefthymiou, Nano Today **4**, 438 (2009).

[13] Wahajuddin and S. Arora, Int. J. Nano Med. **7**, 3445 (2012).

[14] A. Sahoo and D. Bhattacharya, J. Alloys Compd. **772**, 193 (2019).

[15] T. J. Park, G. C. Papaefthymiou, A. J. Viescas, Y. Lee, H. Zhou, and S. S. Wong, Phys. Rev. B **82**, 024431 (2010).

[16] J. B. Goodenough, A. Wold, R. J. Arnott, and N. Menyuk, Phys. Rev. **124**, 373 (1961).

[17] A. E. Berkomitz, J. A. Lahut, I. S. Sacobs, and L. M. Levinson, Phys Rev. Lett. **34**, 594 (1975).

[18] B. M. Wang, Y. Liu, P. Ren, B. Xia, K. B. Ruan, J. B. Yi, J. Ding, X. G. Li, and L. Wang, Phys. Rev. Lett. **106**, 077203 (2011).

[19] T. Maity, S. Goswami, D. Bhattacharya, and S. Roy, Phys. Rev. Lett. **110**, 107201 (2013).

[20] J. Saha and R. H. Victora, Phys. Rev. B **76**, 100405(R) (2007).

[21] F. Radu, M. Etzkorn, R. Siebrecht, T. Schmitte, K. Westerholt, and H. Zabel, Phys. Rev. B **67**, 134409 (2003).

[22] U. P. M. Rasi, N. K. Shihab, S. Angappane, and R. B. Ganginen, Ceram. Int. **45**, 15171 (2019).

[23] J. Nogues and I. K. Schuller, J. Magn. Magn. Mater. **192**, 203 (1999).

[24] M. Ali, P. Adie, C. H. Marrows, D. Greig, B. J. Hickey, and R. L. Stamps, Nat. Mater. **6**, 70 (2007).

[25] J. Nogues, D. Lederman, T. J. Moran, and I. K. Schuller, Phys. Rev. Lett. **76**, 4624 (1996).

[26] O. Iglesias, X. Batlle, and A. Labarta, Phys. Rev. B **72**, 212401 (2005).

[27] S. Chandra, H. Khurshid, M. H. Phan, and H. Srikanth, Appl. Phys. Lett. **101**, 232405 (2012).

[28] Q. K. Ong, A. Wei, and X. M. Lin, Phys. Rev. B **80**, 134418 (2009).

[29] E. C. Sousa, H. R. Rechenberg, J. Depeyrot, J. A. Gomes, R. Aquino, F. A. Tourinho, V. Dupuis, and R. Perzynski, J. Appl. Phys. **106**, 093901 (2009).

[30] M. Sparks, Phys. Rev. Lett. **22**, 1111 (1969).

[31] Z. Nehme, Y. Labaye, R. Sayed Hassan, N. Yaacoub, and J. M. Greneche, AIP Adv. **5**, 127124 (2015).

[32] N. D. Mermin and H. Wagner, Phys. Rev. Lett. **17**, 1133 (1966).

[33] M. Vasilakaki, K. N. Trohidou, and J. Nogues, Sci. Rep. **5**, 9609 (2015).

[34] To obtain hysteresis, the temperature must be lower than the critical value T_c; here $\beta^{-1} = 1$ is much smaller than $T_c = \frac{2}{\ln(1+\sqrt{2})}$ of an Ising model on a square lattice with interaction strength $J = 1$.

[35] R. Wu, S. Ding, Y. Lai, G. Tian, and J. Yang, Phys. Rev. B **97**, 024428 (2018).

[36] E. Eftaxias and K. N. Trohidou, Phys. Rev. B **71**, 134406 (2005).

[37] A. Zaim and M. Kerouad, Physica A (Amsterdam) **389**, 3435 (2010).

[38] X. Sun, N. F. Huls, A. Sigdel, and S. Sun, Nano Lett. **12**, 246 (2012).

[39] B. Khodashenas and H. R. Ghorbani, Arab. J. Chem. **12**, 1823 (2019); J. Helmlinger, C. Sengstock, C. Groß-Heitfeld, C. Mayer, T. A. Schildhauer, M. Köller, and M. Epple, RSC Adv. **6**, 18490 (2016).

[40] Y. Zhao, Y. Wang, F. Ran, Y. Cui, C. Liu, Q. Zhao, Y. Gao, D. Wang, and S. Wang, Sc. Rep. **7**, 4131 (2017).

[41] A. J. Champion, Y. K. Katare, and S. Mitragotri, PNAS **104**, 11901 (2007); W. Zhang, R. Singh, N. Bray-Ali, and S. Haas, Phys. Rev. B **77**, 144428 (2008).

[42] H. Jia, W. Xu, J. An, D. Li, and B. Zhao, Spectrochim. Acta. A. Mol. Biomol. Spectrosc. **64**, 956 (2006).

[43] C. A. Little, C. B. McAuley, N. P. Young, and R. G. Compton, Nanoscale **10**, 15943 (2018).

[44] Q. Song and Z. J. Zhang, J. Am. Chem. Soc. **126**, 6164 (2004).

[45] J. Zwara, E. Grabowska, T. Klimczuk, W. Lisowski, and A. Z. Medynska, J. J. Photochem. Photobiol. A **367**, 240 (2018).

[46] E. A. Kwizera, E. Chaffin, X. Shen, J. Chen, Q. Zou, Z. Wu, Z. Gai, S. Bhana, R. O'Connor, L. Wang, H. Adhikari, S. R. Mishra, Y. Wang, and X. Huang, J. Phys. Chem. C Nanomater Interfaces **120**, 10530 (2016).

[47] J. Hu, S. Zhan, X. Wu, S. Hu, S. Wua, and Y. Liu, RSC Adv. **8**, 21505 (2018).

[48] M. Gibertini, M. Koperski, A. F. Morpurgo, and K. S. Novoselov, Nat. Nanotech. **14**, 408 (2019).